PNAS RESEARCH ARTICLE | NEUROSCIENCE

Energy-efficient network activity from disparate circuit parameters

Michael Deistler[a], Jakob H. Macke[a,b,1,2], and Pedro J. Gonçalves[a,c,1,2]

Edited by Terrence Sejnowski, Salk Institute for Biological Studies, La Jolla, CA; received May 5, 2022; accepted September 19, 2022

Neural circuits can produce similar activity patterns from vastly different combinations of channel and synaptic conductances. These conductances are tuned for specific activity patterns but might also reflect additional constraints, such as metabolic cost or robustness to perturbations. How do such constraints influence the range of permissible conductances? Here we investigate how metabolic cost affects the parameters of neural circuits with similar activity in a model of the pyloric network of the crab *Cancer borealis*. We present a machine learning method that can identify a range of network models that generate activity patterns matching experimental data and find that neural circuits can consume largely different amounts of energy despite similar circuit activity. Furthermore, a reduced but still significant range of circuit parameters gives rise to energy-efficient circuits. We then examine the space of parameters of energy-efficient circuits and identify potential tuning strategies for low metabolic cost. Finally, we investigate the interaction between metabolic cost and temperature robustness. We show that metabolic cost can vary across temperatures but that robustness to temperature changes does not necessarily incur an increased metabolic cost. Our analyses show that despite metabolic efficiency and temperature robustness constraining circuit parameters, neural systems can generate functional, efficient, and robust network activity with widely disparate sets of conductances.

energy efficiency | neuronal variability | neural dynamics | simulation-based inference | Bayesian inference

Neural activity arises from the interplay of mechanisms at multiple levels, including single-neuron and network mechanisms. Several experimental and theoretical studies have found that neural systems can produce similar activity from vastly different membrane and synaptic conductances (1–6), a property sometimes referred to as parameter degeneracy (7, 8). Such parameter degeneracy has been argued to be a prerequisite for natural selection (7) and translates into potential mechanisms of compensation for perturbations of the systems' parameters (3, 5, 9–14). However, in addition to a specific target activity, neural systems are likely subject to additional constraints such as the requirement to be energy efficient (15–17). In order to understand experimentally observed variability and probe potential compensation mechanisms in functioning neural systems, it is thus crucial to characterize the extent of the systems' parameter degeneracy under such additional constraints.

Neuronal activity accounts for the majority of the energy consumed by the brain (18–20). Energy is stored in the ionic gradients across the cell membrane and consumed mostly by action potentials and synaptic mechanisms. Maintaining the ionic gradients requires the action of ion pumps, which consume ATP (15, 21). Previous work has investigated the metabolic efficiency in small neural systems, often at the single-neuron level and with few ion channels (often sodium, potassium, and leak) (15, 22, 23). In these studies, it has been demonstrated that energy consumption of single neurons can be reduced by tuning maximal conductances or time constants of gating variables, while maintaining electrophysiological characteristics, e.g., spike width. However, questions regarding energy efficiency of neural systems remain: First, it is unclear whether previous findings in single neurons (24–26) extrapolate to neural circuits with a large diversity of membrane and synaptic currents (12, 21, 27). Second, the question of how strongly metabolic constraints impact parameter degeneracy remains unaddressed: are energy efficient solutions confined in parameter space, or can disparate network parameters generate energy efficient activity? Last, metabolic cost is only one of many constraints under which neural circuits operate, and it is often unknown whether energy efficiency trades off with other constraints [for a study of how energy efficiency trades off with temperature robustness in a single neuron model of the grasshopper, see Roemschied et al. (28)].

Here we investigate how energy efficiency constrains the parameter degeneracy in the pyloric network in the stomatogastric ganglion of the crab *Cancer borealis* (29, 30), a canonical example of a neural system with parameter degeneracy (5). The pyloric

Significance

Neural systems have the remarkable feature of showing similar activity patterns despite having disparate underlying mechanistic properties (e.g., different ion channel densities). This feature, called parameter degeneracy, underlies the capacity of neural systems to compensate for perturbations to their components. Less understood is whether parameter degeneracy is reduced (or eliminated) by biological constraints, notably to preserve metabolic efficiency or robustness to environmental fluctuations. Developing machine learning methods for degeneracy analysis, we investigated this question in a computational model of the pyloric circuit in the crab stomatogastric ganglion. We found that this circuit can generate functional, energy-efficient, and temperature-robust activity with widely disparate sets of membrane and synaptic conductances. This approach could be exploited beyond the current system.

Author contributions: M.D., J.H.M., and P.J.G. designed research; M.D., J.H.M., and P.J.G. performed research; M.D. contributed new reagents/analytic tools; M.D. analyzed data; and M.D., J.H.M., and P.J.G. wrote the paper.

The authors declare no competing interest.

This article is a PNAS Direct Submission.

Copyright © 2022 the Author(s). Published by PNAS. This article is distributed under Creative Commons Attribution-NonCommercial-NoDerivatives License 4.0 (CC BY-NC-ND).

[1]J.H.M. and P.J.G. contributed equally to this work.

[2]To whom correspondence may be addressed. Email: jakob.macke@uni-tuebingen.de or pedro.goncalves@uni-tuebingen.de.

This article contains supporting information online at https://www.pnas.org/lookup/suppl/doi:10.1073/pnas.2207632119/-/DCSupplemental.

Published October 24, 2022.

Downloaded from https://www.pnas.org by MAX-PLANCK-INSTITUT - FUER on January 24, 2023 from IP address 195.37.61.2.

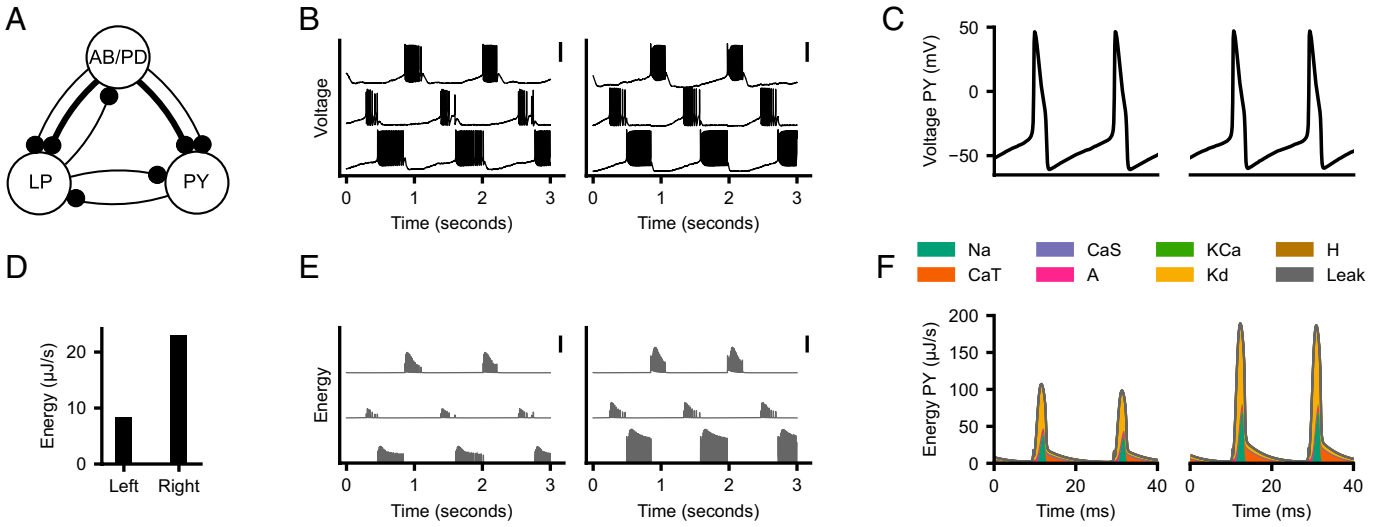

Fig. 1. Similar activity with different energy consumption. (*A*) Computational model of the pyloric network consisting of three model neurons (AB/PD, LP, and PY) and seven synapses. (*B*) Two model configurations with similar circuit activity (traces from top to bottom, AB/PD, LP, and PY) despite different circuit parameters (parameter values not plotted). (Scale bars, 50 mV.) (*C*) Close-up of two spikes in the PY neural activity shown in *B*. (*D*) Total energy consumption divided by the duration of the simulation (10 s) for the traces shown in *B*. The left circuit has threefold lower metabolic cost than the right circuit. (*E*) Consumed energy at each time point. (Scale bar, 100 μJ/s.) (*F*) Energy consumed by each of the ion currents during the two spikes shown in *C* (stacked vertically).

network produces a triphasic motor pattern and consists of a pacemaker kernel (anterior burster neuron [AB] and two pyloric dilator neurons [PD]), as well as two types of follower neurons (a single lateral pyloric [LP] and several pyloric [PY] neurons), interconnected by inhibitory synapses. A model of this circuit with three model neurons (AB/PD, LP, and PY), each with eight membrane currents, and seven inhibitory synapses (Fig. 1*A*; details in *SI Appendix*, SI Text) has been shown to be capable of producing similar network activity with widely different parameters (5).

We start by characterizing the parameter degeneracy of this model: We apply a recently introduced machine learning tool for simulation-based inference, sequential neural posterior estimation (SNPE) (14), to estimate the full set of membrane and synaptic conductances for which the model reproduces experimentally measured electrophysiological activity. We reduce the number of model simulations required to run SNPE by introducing an additional classifier which detects and rejects parameter combinations that produce nonbursting model outputs (31). After characterizing the parameter degeneracy in the model, we show that disparate circuit configurations can have different energy consumption despite similar activity. However, a significant parameter degeneracy is present in the model even when enforcing circuits to have both similar activity and low energy consumption. Furthermore, energy consumption is linearly predictable from circuit parameters, allowing us to identify tuning mechanisms for low metabolic cost. We then show that individual neurons in the pyloric network can be tuned separately to minimize their energy consumption and thereby achieve low energy consumption at the circuit level. Finally, since the crab *C. borealis* is subject to daily and seasonal fluctuations in temperature, we study the trade-off between metabolic cost and robustness to changes in temperature (32–35). We find that metabolic cost can vary across temperatures but that the pyloric network can produce functional, energy-efficient, and temperature-robust activity with disparate parameters.

Results

Disparate Energy Consumption despite Similar Network Activity. We studied the metabolic cost in a model of the pyloric network (Fig. 1*A*). In this model, disparate sets of maximal membrane and synaptic conductances can give rise to similar network activity (5). As an example, we simulated two such circuit configurations (Fig. 1*B*) and computed their metabolic cost using a previously described measure of energy consumption (36). In this measure, the energy for each ion channel is the time integral of the product of the membrane current and the respective difference between the membrane voltage and the reversal potential (details in *SI Appendix*, SI Text). The energy consumed by the entire neural circuit is the sum of the energies across channels of all neurons. We note that this power-based energy measure likely underestimates the true energy consumption but is strongly correlated with the current-based energy measure based on sodium and calcium currents (15, 25) (*SI Appendix*, Figs. S1 and S2). Since the power-based measure naturally allows us to quantify the energy consumed by a larger diversity of currents, we performed our main analyses with this measure, although our main results are maintained when using the current-based measure (*SI Appendix*, Fig. S3).

Although the two simulated circuit configurations produce similar network activity, even at the single-spike level (Fig. 1*C*), the total energy consumption (Fig. 1*D*) as well as the moment by moment energy consumption differ substantially (Fig. 1*E*). A closer inspection of the energy consumed by each current in the PY neuron during the action potentials (37) shows that the difference in energy between these two network configurations is also evident in the energy consumed by the sodium current Na, the delayed-rectifier potassium current K_d, and the transient calcium current CaT (Fig. 1*F*).

Disparity in Energy Consumption in Models Matching Experimental Data. The example above illustrates that the model of the pyloric network can, in principle, produce the same activity with different metabolic costs. However, it is unclear how broad the range of metabolic costs associated with the same network output is. In order to address this, we need to identify the full space of maximal membrane and synaptic conductances (31 parameters in total) that match experimental measurements of network activity and to characterize the energy consumption of each of these configurations.

We used a recently introduced machine learning tool for simulation-based inference, SNPE (14), to estimate the set of circuit parameters (the posterior distribution) consistent with data

Downloaded from https://www.pnas.org by MAX-PLANCK-INSTITUT - FUER on January 24, 2023 from IP address 195.37.61.2.

and prior assumptions about the parameters. In SNPE, parameters which specify network configurations are initially sampled from the prior distribution (in our case, a uniform distribution within plausible parameter ranges) and used to simulate network activity. Subsequently, a neural network–based density estimator is trained on these simulated network activities to learn which parameter sets produce network activity that is compatible with empirical observations.

In order to generate the training data for the neural network, SNPE requires millions of model simulations to accurately infer the set of data-compatible parameters. To improve the simulation efficiency and make the neural network predict parameter sets that more closely match experimental data, we introduced a modification of the algorithm (Fig. 2*A*). Specifically, a technical challenge for SNPE is that parameter sets sampled from the prior distribution might produce simulation results that are not valid, i.e., produce clearly nonsensible data: for example, if there are no bursts, phase gaps between bursts are not defined (Fig. 2*A*, fourth panel, red). For SNPE, these invalid simulations are discarded immediately. In order to reduce the fraction of simulations that are discarded, we introduce a classifier to predict whether a parameter set will lead to a valid or an invalid simulation output (31) (Fig. 2*A*, second panel). Once the classifier is trained on an initial set of simulations, parameters are immediately discarded without running the simulation, if the classifier confidently predicts that the simulation will be invalid (details in *SI Appendix*, SI Text). We name the distribution of parameters that are accepted by the classifier the "restricted prior" (Fig. 2*A*, third panel). Once sufficiently many valid simulations are performed, SNPE proceeds by training a deep neural density estimator to estimate the posterior distribution over parameters of the model (14) (Fig. 2*A*, fifth and sixth panels; proof of convergence to the correct posterior distribution in *SI Appendix*, SI Text).

We used this procedure to infer the posterior distribution over maximal membrane and synaptic conductances of the model of the pyloric network given salient and physiologically relevant features of experimentally measured data. These features are the cycle period, burst durations, duty cycles, phase gaps, and phase delays of the triphasic rhythm (Fig. 2*B*; details in *SI Appendix*, SI Text) (38). As in previous studies (4, 5), we did

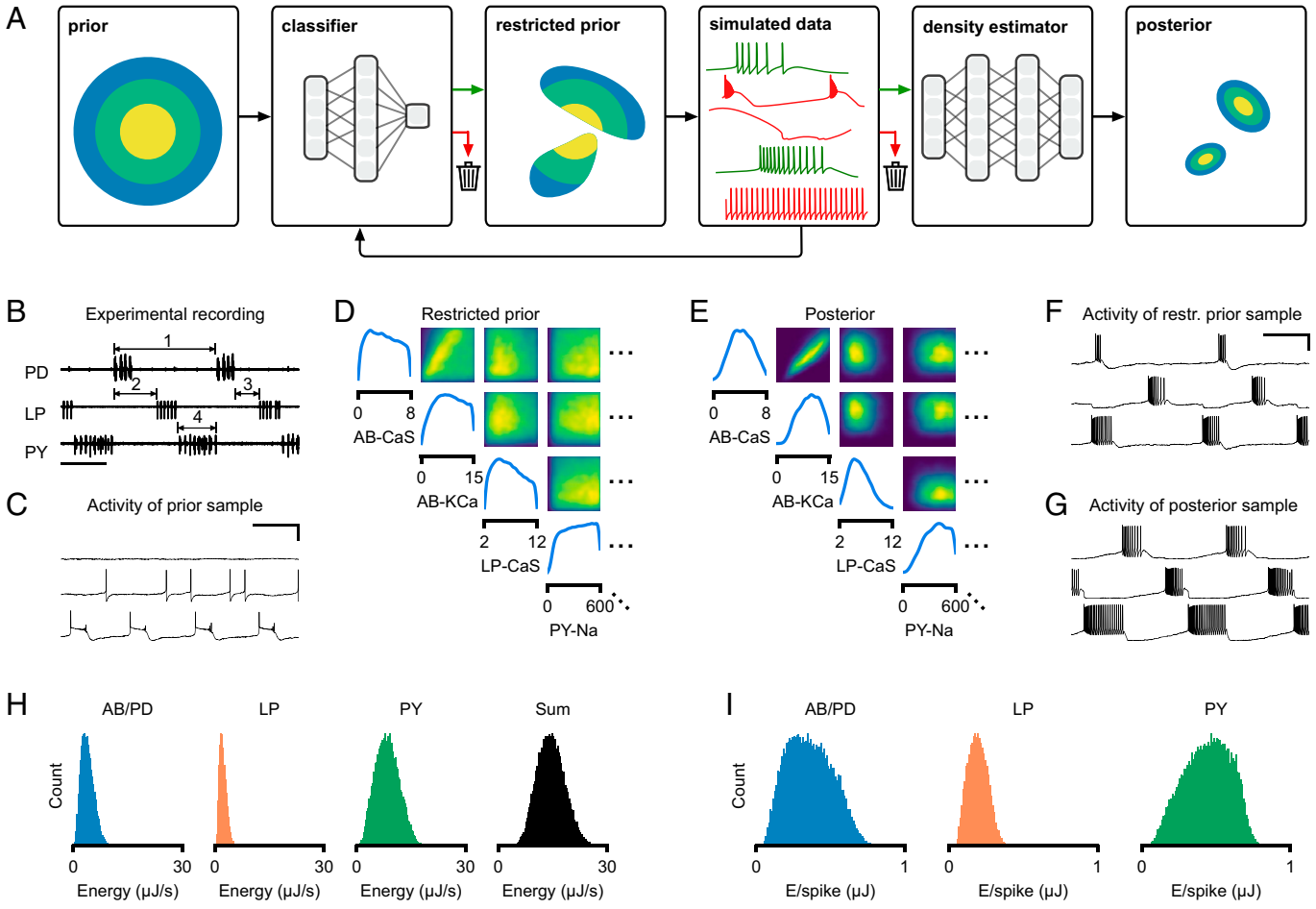

Fig. 2. Bayesian inference reveals wide range of energy consumption. (*A*) Inferring the posterior distribution by combining a rejection classifier and a deep neural density estimator. First, a classifier (trained on an initial set of simulations) predicts which circuit parameters sampled from the prior produce valid simulation outputs. We then proceed by sampling from the part of the parameter space that is accepted by the classifier, i.e., the restricted prior. All valid data (green) are used to train a deep neural density estimator, and all invalid data are discarded (red) (14). Once this estimator is trained, it can be evaluated on experimental data to return the posterior distribution over model parameters. (*B*) Experimental data recorded from the pyloric network (38). Arrows indicate a subset of the physiologically relevant features, namely, the cycle period (arrow 1), phase delays (arrow 2), phase gaps (arrow 3), and burst durations (arrow 4) (see *SI Appendix*, SI Text for details). (Scale bar, 500 ms.) (*C*) Simulation output from a parameter set sampled from the prior distribution. The traces are AB/PD (*Top*), LP (*Middle*), and PY (*Bottom*). (Scale bars, 500 ms and 50 mV.) (*D*) Subset of the marginals and pairwise marginals of the 31-dimensional restricted prior, i.e., the subspace of parameters for which the model produces bursting activity. All maximal conductances are given in mS/cm^2. (*E*) Subset of the marginals and pairwise marginals of the posterior distribution, i.e., the subspace of parameters for which the model matches experimental data shown in *B* (full posterior distribution in *SI Appendix*, Fig. S13). (*F*) Sample from the restricted prior producing bursting activity but not matching experimental data. (*G*) Sample from the posterior distribution closely matching features of the experimental data. (*H*) Histograms over energy consumed by each neuron (blue, orange, and green) as well as by the entire circuit (black), divided by the duration of the simulation. Trace with lowest energy consumes nine times less energy than trace with highest energy. (*I*) Same as in *H* but for energy per spike.

Downloaded from https://www.pnas.org by MAX-PLANCK-INSTITUT - FUER on January 24, 2023 from IP address 195.37.61.2.

not constrain the model of the pyloric network by the number of spikes or the spike shapes. Below, we describe the results obtained for a specific experimental preparation. We qualitatively reproduced all results with two additional experimental preparations (*SI Appendix*, Figs. S4–S9) (38). We note that SNPE captures parameter uncertainty stemming from epistemic uncertainty as well as from nonidentifiability of parameters (i.e., parameter degeneracy). Given that the experimentally measured voltage traces contain little variability between different cycles of the triphasic rhythm (*SI Appendix*, Fig. S10), we introduced a modest amount of current noise in the pyloric network model (*SI Appendix*, Fig. S11; details in *SI Appendix*, SI Text). Thus, the epistemic uncertainty of the inference is small, and posterior uncertainty is likely dominated by parameter degeneracy. Further evidence of this is the fact that different noise sources do not significantly affect posterior variability (*SI Appendix*, Fig. S12).

When simulating the pyloric network model with parameter sets sampled from the prior distribution, 99% of simulations do not produce spikes or bursts, and hence, characteristic summary features of the circuits are not defined (Fig. 2*C*). The restricted prior (Fig. 2*D*) is narrower than the prior distribution but considerably broader than the posterior (Fig. 2*E*; full posterior distribution in *SI Appendix*, Fig. S13; comparison between prior, restricted prior, and posterior in *SI Appendix*, Fig. S14). Parameters sampled from the restricted prior often produce activity with well-defined summary features (Fig. 2*F*) but do not generally match experimental data, whereas samples from the posterior closely match experimental data (Fig. 2*G*). By using the classifier to reject invalid simulations, we required half as many simulations compared to classical SNPE (14) and achieved a higher accuracy (*SI Appendix*, Fig. S15). For the subsequent analyses, we only considered posterior samples whose activity was within a prescribed distance to the experimental data and discarded all other samples (details in *SI Appendix*, SI Text). We simulated 1 million parameter configurations sampled from the posterior, out of which ∼3.5% fulfilled the distance criterion, leading to a database of 35,939 parameter sets whose activity closely matched experimental data. Sampling from the prior distribution rather than the posterior would have required ∼600 billion simulations to obtain 35,939 parameter sets that fulfill our criterion (60,000 times more than with our method).

We computed the energy consumption of each of the 35,939 circuit activities (Fig. 2*H*). The circuit configuration with lowest total energy consumes nine times less energy than the circuit configuration with highest total energy. To ensure that the difference in energy does not only stem from different numbers of spikes within a burst, we also computed the average energy consumed during a spike (energy per spike) in each of the neurons (Fig. 2*I*). As with total energy, energy per spike strongly varies across parameter configurations. We note that the differences between the individual neurons might in part be attributed to the different prior ranges of maximal conductances across neurons [ranges based on results from Prinz et al. (5); *SI Appendix*, SI Text]. These results show that despite similar circuit function, different parameter sets can have vastly different energy consumption. Below, we investigate the mechanisms giving rise to this phenomenon.

Metabolic Constraints on Individual Circuit Parameter Ranges. How strongly does enforcing low energy consumption constrain the permissible ranges of circuit parameters? We inspected the circuit parameters of the 2% most and least efficient configurations within our database of 35,939 model configurations (Fig. 3 *A*, *Left*). For some circuit parameters, the range of values producing efficient activity is clearly different from the range of

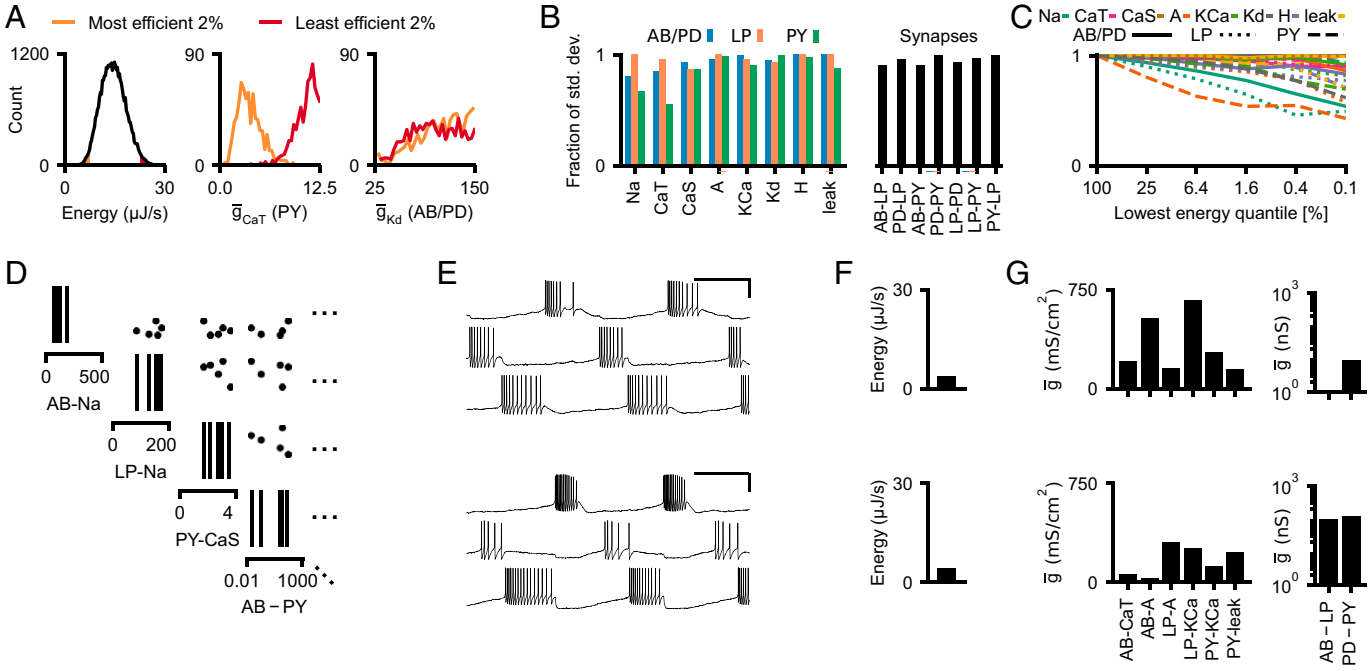

Fig. 3. Metabolic constraints on individual circuit parameters. (*A*) (*Left*) Time-averaged energy consumption of 35,939 models that match experimental data. The orange area corresponds to the energy consumption in the lowest 2% quantile, and the red area corresponds to the top 98% quantile. (*Middle*) Distribution of the maximal conductance of the transient calcium channel (CaT) in the PY neuron in the 2% (orange) and 98% quantile (red). (*Right*) Distribution of the maximal conductance of the delayed-rectifier potassium channel (K_d) in the AB/PD neuron in the 2% (orange) and 98% quantile (red). (*B*) SD of parameters for models with energy consumption in the lowest 2% quantile. SD is normalized to the SD of the parameters across all 35,939 models in our database. (*C*) Same as *B* but for a range of quantiles. Solid, AB/PD; dotted, LP; dashed, PY. Colors are the same as in Fig. 1*F*. Synapses are in *SI Appendix*, Fig. S18. (*D*) Subset of the parameter values of the five most efficient circuit configurations in our database. (*E*) The network activity produced by two of these five configurations. (Scale bar, 500 ms and 50 mV.) (*F*) Time-averaged energy consumption of the two configurations shown in *D*. (*G*) Subset of circuit parameters of the two solutions shown in *B*. Despite similar network activity and low energy consumption, several parameters differ by more than twofold. The membrane conductances are scaled by the following factors (left to right): 100, 10, 10, 100, 100, and 10,000.

Downloaded from https://www.pnas.org by MAX-PLANCK-INSTITUT - FUER on January 24, 2023 from IP address 195.37.61.2.

values producing energetically costly activity (e.g., the maximal conductance of the transient calcium current in the PY neuron; Fig. 3 *A*, *Middle*). For other parameters, the range does not change (e.g., the maximal conductance of the delayed-rectifier potassium current in the AB/PD neuron; Fig. 3 *A*, *Right*). To quantify how strongly low energy consumption constrains parameters, we compared the parameter SD across all 35,939 model configurations to that of the most efficient 2% (Fig. 3 *B* and *C*; *SI Appendix*, Fig. S16 show how the parameter means shift as energy constraints are enforced). Most parameters in the circuit barely get constrained by energy consumption (values close to 1 in Fig. 3 *B* and *C*). The parameters that get constrained the most by enforcing low energy consumption are the Na and CaT conductances of the AB/PD neuron; the CaS conductance of the LP neuron; and the Na, CaT, CaS, and leak conductances of the PY neuron. However, for all of these parameters, a large fraction of variability remains. In addition, we found that enforcing energy constraints affects correlations between parameters only weakly (*SI Appendix*, Fig. S17).

In order to ensure that the remaining variability of circuit parameters does not stem from the remaining variability of energy consumptions within the lowest 2% quantile, we inspected the five most efficient configurations in our database of 35,939 model configurations. Even these five circuit configurations have strongly disparate circuit parameters (Fig. 3*D*). Despite having similar activity (Fig. 3*E*) and very low (and similar) metabolic cost (Fig. 3*F*), their circuit parameters are disparate (Fig. 3*G*). These results demonstrate that metabolic efficiency constrains the range of some circuit parameters, but it is possible to achieve low metabolic cost and similar network activity with widely disparate circuit parameters.

Sodium and Calcium Conductances Influence Energy Consumption Most Strongly. We wanted to understand how each circuit parameter affects energy consumption within our database of 35,939 model configurations. Given that the voltage wave forms of the model configurations within our database are constrained to be similar, energy consumption is expected to be approximately linearly related to the maximal conductances (*SI Appendix*, SI Text). We, therefore, performed a linear regression $E = w^T\theta + b$ from circuit parameters (taken from our database of 35,939 model configurations) onto the energy consumption of these circuits (Fig. 4*A*; details in *SI Appendix*, SI Text). This linear regression achieved a high accuracy, demonstrating that energy consumption can indeed be linearly predicted from circuit parameters (Fig. 4*B*; a nonlinear regression with a neural network leads to similar results and is shown in *SI Appendix*, Fig. S19; details in *SI Appendix*, SI Text). The regression weights w indicate how strongly energy consumption is correlated with each parameter value (Fig. 4*C*). The maximal sodium conductances $\overline{g}_{\mathrm{Na}}$, transient calcium conductances $\overline{g}_{\mathrm{CaT}}$, and slow calcium conductances $\overline{g}_{\mathrm{CaS}}$ are most strongly correlated with energy consumption: increases of these conductances are associated with an increase in energy consumption, and thus, small conductance values correspond to metabolically more efficient solutions. The membrane conductances of the PY neuron influence energy consumption more strongly than the LP and AB/PD neurons. This is expected since the PY model neuron consumes more energy than the other neurons (Fig. 2*H*). The synaptic conductances are weakly correlated with energy consumption, which can be explained by the low values of the maximal synaptic conductances: the synaptic strengths range up to 1,000 nS, whereas the membrane conductances can range

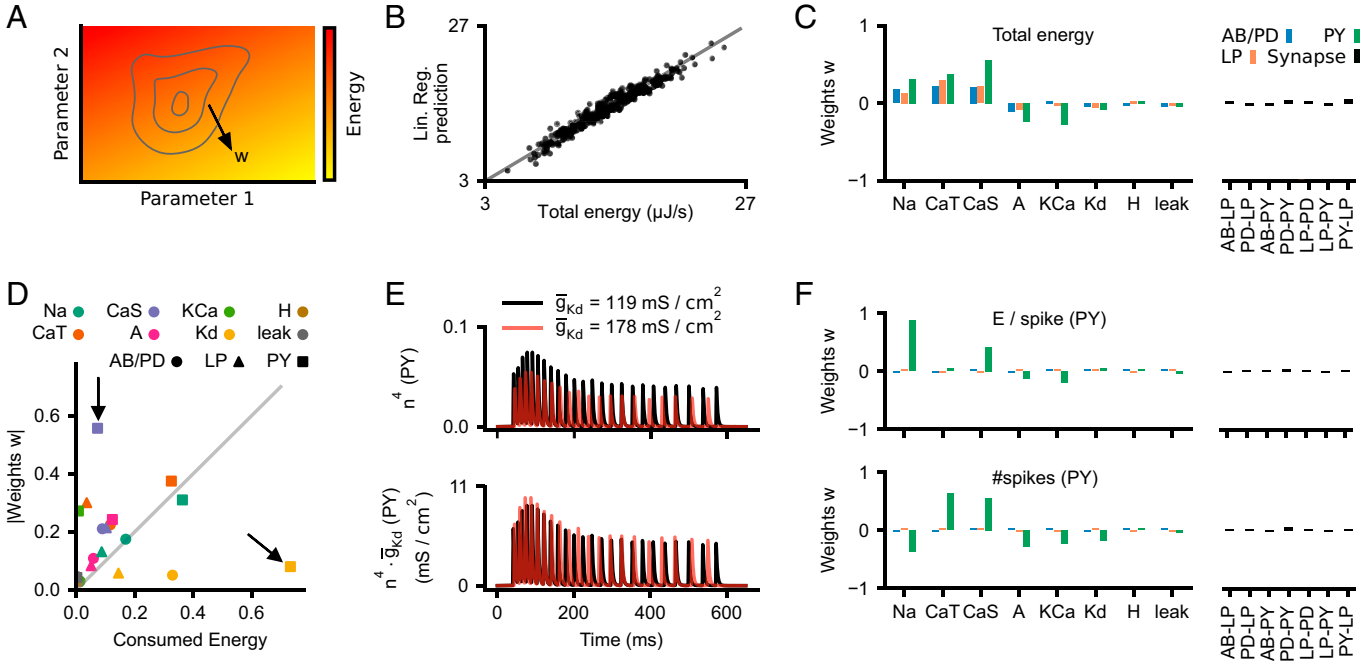

Fig. 4. Influence of circuit parameters on energy consumption. (*A*) Illustration of the energy landscape under functional constraints (matching experimental activity). The linear regression weights correspond to the direction along which energy varies. (*B*) The linear regression accurately predicts the energy consumption on a test set of 300 circuit configurations (black dots). Gray line is the identity function. (*C*) Weights *w* of the linear regression. (*Left*) Weights of the maximal membrane conductances. (*Right*) Weights of the maximal synaptic conductances. (*D*) Weights *w* as a function of energy consumption (both normalized), for all membrane currents (arrows highlight two illustrative examples). Membrane conductances on the top left consume little energy, but their maximal conductances correlate strongly with energy consumption. Conductances on the bottom right consume a lot of energy, but their maximal conductances correlate weakly with energy consumption. (*E*) (*Top*) The gating variable n^4 of the K_d current in the PY neuron during activity produced by two circuit configurations (black and red), which are identical apart from the magnitude of $\overline{g}_{\mathrm{Kd}}$. (*Bottom*) The product of gating variable and maximal conductance $n^4 \cdot \overline{g}_{\mathrm{Kd}}$ for the same configurations. (*F*) (*Top*) Weights of a linear regression onto the energy per spike in the PY neuron. (*Bottom*) Weights of a linear regression onto the number of spikes in the PY neuron.

Downloaded from https://www.pnas.org by MAX-PLANCK-INSTITUT - FUER on January 24, 2023 from IP address 195.37.61.2.

up to 0.4 mS (i.e., 4×10^5 nS), such that synapses consume only 0.08% of the total energy in the circuit. These results demonstrate that energy consumption can be linearly predicted from circuit parameters and that energy consumption is most strongly correlated with the maximal conductances of sodium as well as slow and transient calcium.

How do different currents affect total energy consumption? Do they directly consume energy, or do they trigger processes that then require energy? We addressed these questions by comparing the fraction of energy consumed by each current [as defined by our measure of energy (36); Fig. 1*F*] to the linear regression weight w associated with its maximal conductance (Fig. 4*D*). We found that some currents consume a lot of energy, although their maximal conductances barely correlate with energy consumption, e.g., the K_d current in the PY neuron (Fig. 4*D*, bottom right arrow), while other currents consume little energy, but nonetheless their maximal conductances are correlated with energy consumption, e.g., the CaS current of the PY neuron (Fig. 4*D*, top left arrow).

We investigated the neuronal mechanisms that give rise to these behaviors. First, to understand how currents can consume large amounts of energy despite their maximal conductance only weakly correlating with energy, we investigated the effects of the delayed-rectifier potassium conductance $\overline{g}_{\mathrm{Kd}}$ on circuit activity. We simulated two circuit configurations, identical apart from the magnitude of $\overline{g}_{\mathrm{Kd}}$ in the PY model neuron. In the configuration with higher $\overline{g}_{\mathrm{Kd}}$, the gating variable n did not reach values as high as those for the other configuration, thus leading to a similar effective conductance $n^4 \cdot \overline{g}_{\mathrm{Kd}}$ (Fig. 4*E*). This demonstrates that changes in the maximal conductance $\overline{g}_{\mathrm{Kd}}$ only weakly influence the current and thereby the energy consumption. Thus, despite the potassium current consuming a lot of energy due to a large flow of ions (compared to other channels), its maximal conductance $\overline{g}_{\mathrm{Kd}}$ only weakly correlates with energy consumption.

Second, to understand how maximal conductances can correlate with energy consumption despite their channels consuming little energy, we disentangled the correlation of circuit parameters with energy consumption into two parts: the energy per spike and the number of spikes. We fitted two additional linear regression models: one regression from circuit parameters onto number of spikes in the PY neuron and one regression from circuit parameters onto energy per spike in the PY neuron. We again found good predictive performance of these models, showing that the energy per spike and the number of spikes can also be linearly predicted from circuit parameters (regression performance in *SI Appendix*, Fig. S20). The energy per spike is strongly correlated with the sodium conductance (Fig. 4 *F*, *Top*), whereas the number of spikes is most strongly correlated with the maximal conductance of transient and slow calcium (Fig. 4 *F*, *Bottom*). This demonstrates that increases in the maximal conductance of calcium lead to a higher number of spikes, which involve increased energy consumption through other currents. We verified this hypothesis by simulating two configurations that were identical apart from the magnitude of $\overline{g}_{\mathrm{CaS}}$ in the PY model neuron and found that the configuration with higher $\overline{g}_{\mathrm{CaS}}$ indeed produced more spikes per burst (*SI Appendix*, Fig. S21). This shows that despite the slow calcium channel consuming little energy itself, increasing $\overline{g}_{\mathrm{CaS}}$ can lead to higher energy consumption by increasing the number of spikes, which involve energy consumption through other currents (mostly sodium and potassium). Overall, our analyses demonstrate that currents which consume a lot of energy are not necessarily the ones that influence energy the most.

Minimal Tuning Mechanisms for Low Energy Consumption. We identified circuit parameters that correlate with energy consumption, but this does not yet address the question of which changes of these parameters will lead to the reduction of energy consumption: First, a correlation between parameter values and energy consumption does not imply a causal connection between these. Second, parameters that correlate strongly with energy consumption might have to be finely tuned to match the pyloric rhythm, thus not constituting a feasible substrate for reducing energy consumption. Therefore, we went beyond the previous analysis to investigate potential tuning mechanisms involving single and pairs of parameters that would reduce energy consumption while maintaining the pyloric rhythm.

We investigated how strongly energy consumption could be reduced by mechanisms that involve a single parameter. For instance, we kept all parameters but the maximal sodium conductance of the AB/PD neuron ($\overline{g}_{\mathrm{Na}}$) constant and varied $\overline{g}_{\mathrm{Na}}$ on a grid. We then estimated the energy consumption of each configuration with the previously identified linear model (Fig. 4). The energy consumption of the circuit increases with $\overline{g}_{\mathrm{Na}}$ (Fig. 5*A*), but for too low (or too high) $\overline{g}_{\mathrm{Na}}$, the network activity does not match experimental data (we rejected parameters for which the posterior density is too low; *SI Appendix*, SI Text). Thus, despite $\overline{g}_{\mathrm{Na}}$ strongly correlating with energy consumption (Fig. 4*C*), energy consumption can be reduced only modestly when tuning $\overline{g}_{\mathrm{Na}}$ and keeping all other parameters constant.

We then investigated whether pairwise mechanisms could lead to larger savings in energy consumption. For instance, we kept all parameters but $\overline{g}_{\mathrm{Na}}$ and the delayed-rectifier potassium conductance of the AB/PD neuron ($\overline{g}_{\mathrm{Kd}}$) constant and varied the remaining two parameters on a grid. We estimated the energy consumption of any configuration on this grid and found that the most efficient parameter configuration is 23% more efficient than the most wasteful configuration (Fig. 5*B*). This reduction in energy consumption could be achieved through a simple pairwise mechanism: a reduction of sodium combined with an increase of potassium allows the network to maintain its activity (Fig. 5 *C* and *D*), while reducing the metabolic cost (Fig. 5*B*).

We repeated this analysis for every conductance and every pair of conductances (Fig. 5 *E* and *F*). Note that we only considered pairs of parameters within each neuron because pairwise compensation mechanisms across neurons have been shown to be weak in this model (14). Some of the single-conductance mechanisms can reduce the energy consumption by up to 36%. Pairwise mechanisms, such as reducing the sodium and transient calcium conductances of the PY neuron, can reduce the energy consumption of the entire circuit by up to 55%. When considering only the energy consumed in a specific neuron, pairwise mechanisms can reduce energy consumption by up to 80% (*SI Appendix*, Fig. S22). Finally, pairwise mechanisms between synapses and conductances of the respective postsynaptic neurons can reduce energy consumption of the entire circuit by up to 43%.

These analyses provide hypotheses for causal mechanisms for how neurons can be tuned into low-energy regimes, while the neural activity keeps satisfying functional constraints. We demonstrated that even simple mechanisms involving one or two conductances can have a substantial impact on the energy consumption of the circuit—thus, low-energy configurations can be found with local parameter changes, not requiring fine coordination among multiple parameters.

Neurons Can Be Tuned Individually to Achieve Minimal Circuit Energy. Next, we asked how single neurons interact to produce functional and efficient circuit activity. Can the energy of the entire circuit be minimized by optimizing the energy of each neuron individually? Does the circuit retain functional activity when

Downloaded from https://www.pnas.org by MAX-PLANCK-INSTITUT - FUER on January 24, 2023 from IP address 195.37.61.2.

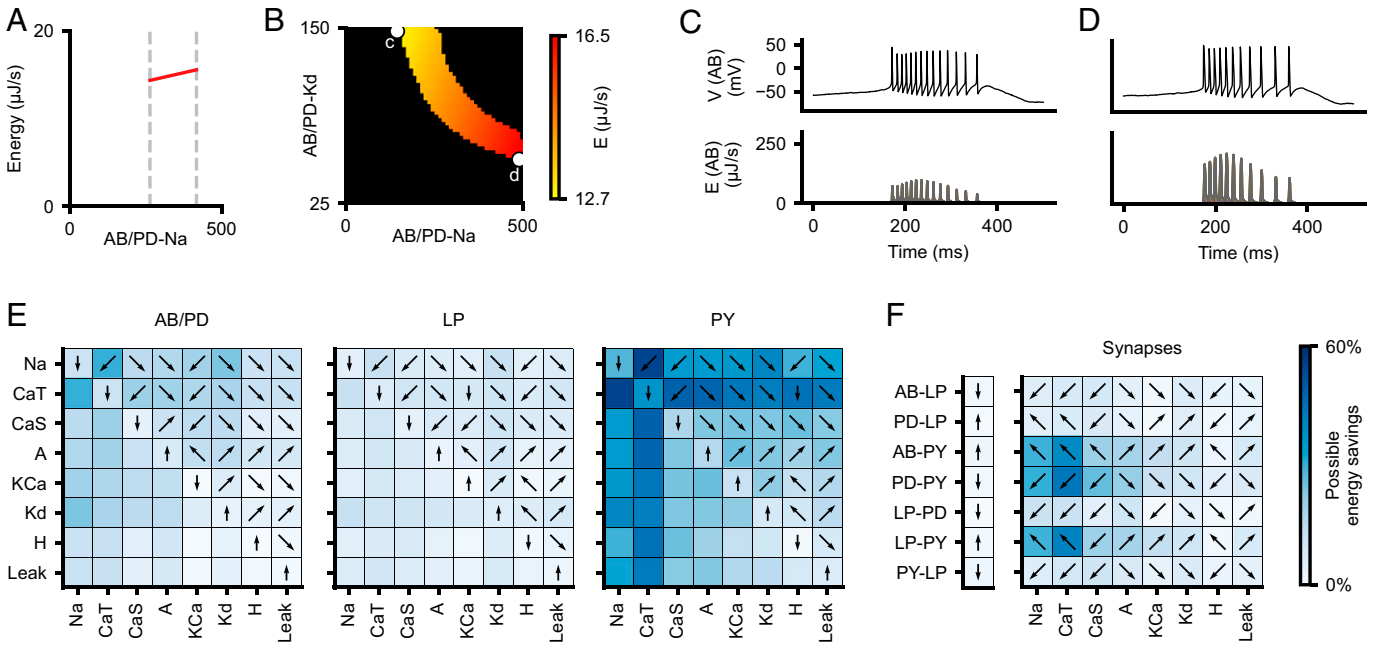

Fig. 5. Minimal tuning mechanisms for low energy consumption. (*A*) Time-averaged energy consumption (as predicted by linear regression) of several models that differ only in their maximal sodium conductance in the AB/PD neuron. Energy increases with $\bar{g}_{Na}$. We excluded circuits with too low and too high values of $\bar{g}_{Na}$, for which the model does not reproduce experimental data. (*B*) Same as *A* but for models that differ in their maximal conductances of sodium (Na) and delayed-rectifier potassium (K_d) in the AB/PD neuron. (*C*) (*Top*) Voltage trace of the AB/PD neuron for the most efficient configuration within the plane shown in *B*. (*Bottom*) Energy consumption during that activity. (*D*) Same as *C* but for the least efficient configuration. (*E*) Fraction of energy that can be saved by modifying a single membrane parameter (diagonal of each matrix) or pairs of membrane parameters (upper and lower diagonal). Color bar is the same as in *F*. Arrows indicate the direction in which (pairs of) parameters should change in order to reduce energy: left/right refers to the parameter on the *x* axis, and top/bottom refers to the parameter on the *y* axis. (*F*) Fraction of energy that can be saved by modifying a synaptic conductance (vector on the left) or the synaptic conductance and one membrane conductance of the respective postsynaptic neuron (matrix on the right).

neurons are individually optimized for low energy efficiency? Within our database of 35,939 model configurations, there is a weak correlation between the energies consumed by pairs of neurons, which suggests that the energy consumption between neurons might be independent from one another (Fig. 6*A*; AB/PD versus LP, correlation coefficient $r = -0.006$, P value $p = 0.23$; LP versus PY, $r = 0.02$, $p = 3 \times 10^{-6}$; AB/PD versus PY, $r = -0.03$, $p = 8 \times 10^{-9}$). We thus investigated whether we could optimize the parameters of each neuron individually for low energy consumption and still retain functional circuit activity. We searched our database of 35,939 model configurations for the single-neuron models with minimal energy consumption individually. We selected the five most efficient single-neuron parameter combinations for each of the neurons and assembled them into 125 (5^3) network configurations. We then identified synaptic conductances that match each of these configurations with Markov chain Monte Carlo (Fig. 6*B*; details in *SI Appendix*, SI Text). Notably, given the already estimated full posterior distribution, this step does not require additional simulations.

For each of the 125 combinations of membrane conductances, we found a set of synaptic conductances for which the network activity closely resembles experimentally measured activity (Fig. 6*C*). The resulting configurations have disparate parameters (Fig. 6*D*) but highly similar network activity. Furthermore, we found that the resulting configurations have similar and very low energy consumption. The energy consumption of these circuits is significantly smaller than that of any of the configurations in our database of 35,939 model configurations (Fig. 6*E*). This demonstrates that optimizing a specific neuron for energy efficiency does not preclude the connected neurons from being energy efficient. Thus, our results suggest that the pyloric network can be optimized for energy efficiency by tuning neurons individually for low energy consumption.

We estimated how likely these energy-efficient circuits are under the estimated posterior. We found that all these models have similar posterior log-probability as the 35,939 model configurations in our database (Fig. 6*F*); i.e., they are part of the inferred posterior and are as likely to underlie the experimentally measured activity as the database models. How, then, are these newly found configurations so much more energy-efficient than configurations sampled from the posterior? Given that the posterior is a high-dimensional distribution (31 dimensions), drawing random samples from such a distribution will unlikely result in configurations for which all three neurons are optimally efficient, and we cannot exclude the possibility that there might be unsampled regions in parameter space with even more energy-efficient circuit configurations.

Robustness to Temperature Does Not Require an Increased Metabolic Cost. The crab *C. borealis* experiences daily and yearly fluctuations in temperature which in turn influence the chemical and physical properties of neurons (32–34). Nonetheless, neural circuits such as the pyloric network can maintain their functionality in the presence of these temperature variations. As temperature increases, the cycle frequency of the circuit increases exponentially, but the phases between bursts remain relatively constant (35, 39). We investigated whether the pyloric network trades off robustness to changes in temperature with energy efficiency, i.e., whether temperature-robust solutions are more energetically costly.

The temperature dependence of a biophysical parameter R is captured by the Q_{10} value and is defined as follows:

$$R_T = R_{ref}\, Q_{10}^{(T - T_{ref})/10},$$

where R_{ref} is the parameter value at the reference temperature $T_{ref} = 11\ ^\circ\mathrm{C}$. We extended the model of the pyloric network to include Q_{10} values for all maximal membrane and synaptic

Downloaded from https://www.pnas.org by MAX-PLANCK-INSTITUT - FUER on January 24, 2023 from IP address 195.37.61.2.

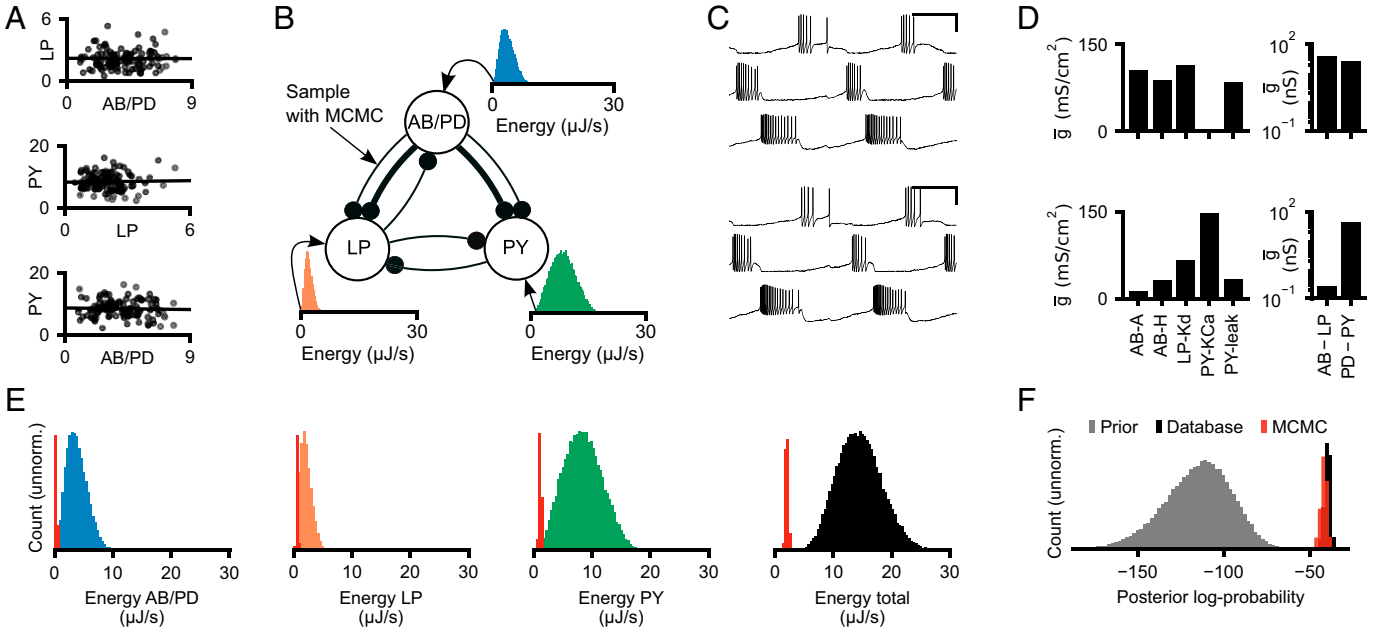

Fig. 6. Neurons can be tuned individually to achieve minimal circuit energy consumption. (*A*) Black dots indicate energy consumed by each neuron separately. Shown are 100 randomly selected parameter configurations from our database of 35,939 configurations. Linear regression (black line) shows a weak correlation between the energy consumed by pairs of neurons. (*B*) We select the five most efficient parameter configurations for each neuron separately and search with Markov chain Monte Carlo for synaptic conductances such that the target circuit activity is achieved. (*C*) The activity produced by two parameter configurations produced with the strategy described in *B*. (*D*) A subset of the (*Left*) membrane and (*Right*) synaptic conductances for the configurations in *C*. Despite generating similar network activity, the configurations have very different circuit parameters. The membrane conductances are scaled with the following factors (left to right): 10, 10,000, 1, 100, and 10,000. (*E*) Histogram over the energy consumption (time averaged) of all 35,939 models in our database (blue, orange, green, and black) and the energy consumption of the configurations produced with the strategy described in *B* (red). (*F*) Histogram of the posterior log-probability for samples from the prior distribution (gray), for the 35,939 models in our database (black), and for the configurations produced with the strategy described in *B* (red).

conductances (details in *SI Appendix*, SI Text) (40, 41). We then used SNPE to identify all maximal membrane and synaptic conductances, as well as the associated Q_{10} values (41 parameters in total) that match experimental recordings at 11 and 27 °C (Fig. 7*A*) (38). We set the previously identified posterior distribution (Fig. 2*E*) over circuit parameters given experimental data at 11 °C as the new prior distribution and then applied SNPE to match the model with experimental data at 27 °C (Fig. 7*B*; full posterior in *SI Appendix*, Fig. S23, and details in *SI Appendix*, SI Text). We sampled circuit parameters and Q_{10} values from the resulting distribution and selected samples whose activity closely matched experimental data at 11 and 27 °C (Fig. 7*C*). Overall, we generated a database of 967 sets of circuit parameters and Q_{10} values. When simulating at temperatures between 11 and 27 °C, these circuits show the characteristic exponential increase in cycle frequency as well as the constant phase relationship between bursts observed experimentally (Fig. 7*D*) (35).

We asked whether the energy consumed by the circuit at 11 °C is proportional to the energy consumed at 27 °C. We found that despite the number of spikes in our model being higher at higher temperatures, the total energy consumption is lower at 27 °C (Fig. 7*E*; note that for one of the three preparations, the energy consumptions at 11 and 27 °C are similar; *SI Appendix*, Fig. S9). This occurs because at higher temperatures, the increase in the number of spikes is accompanied by a decrease in channel time constants and respective decrease in energy per spike (*SI Appendix*, Fig. S24). In addition, there is a clear correlation between energy consumptions at 11 and 27 °C (Pearson correlation coefficient, 0.66), although circuit configurations with similar efficiency at 11 °C can show a range of energy consumptions at 27 °C (Fig. 7*E*).

We then investigated how the additional constraint of temperature robustness impacts the parameter degeneracy of the pyloric network. We computed the SD of the maximal conductances across the models that match experimental data at 11 and 27 °C and whose energy consumption is in the 2% quantile at both temperatures (Fig. 7*F*). The resulting SD is smaller than that of all models in our database of 35,939 models, but a large parameter variability remains. Thus, we found a substantial parameter degeneracy in circuits constrained by "pyloric-ness," energy efficiency, and temperature robustness.

Does temperature robustness have an influence on metabolic cost? We computed the energy consumed at 11 °C for three different scenarios: first, for all models in our database of 35,939 model configurations matching experimental data recorded at 11 °C (same as Fig. 2*H*); second, for all models in our database of 35,939 model configurations that are also functional at 27 °C (i.e., produce triphasic activity); and third, for all models in our database of 967 model configurations matching experimental data recorded at 11 and 27 °C. In all three of these scenarios, the distribution of metabolic cost was similar (Fig. 7*G*; note that the slightly different average energy consumption between the first and the third scenarios occurred only in two of the three preparations; *SI Appendix*, Figs. S6 and S9). In particular, all three scenarios contained configurations that produce energy-efficient circuit function. This demonstrates that enforcing temperature robustness does not require the pyloric network to be less energy efficient.

Overall, our analyses indicate that the model of the pyloric network retains substantial parameter degeneracy despite constraints on energy efficiency and temperature robustness. In addition, we showed that temperature robustness does not entail additional metabolic cost.

Discussion

Neural systems undergo environmental and neuromodulatory perturbations to their mechanisms. The parameter degeneracy

Downloaded from https://www.pnas.org by MAX-PLANCK-INSTITUT - FUER on January 24, 2023 from IP address 195.37.61.2.

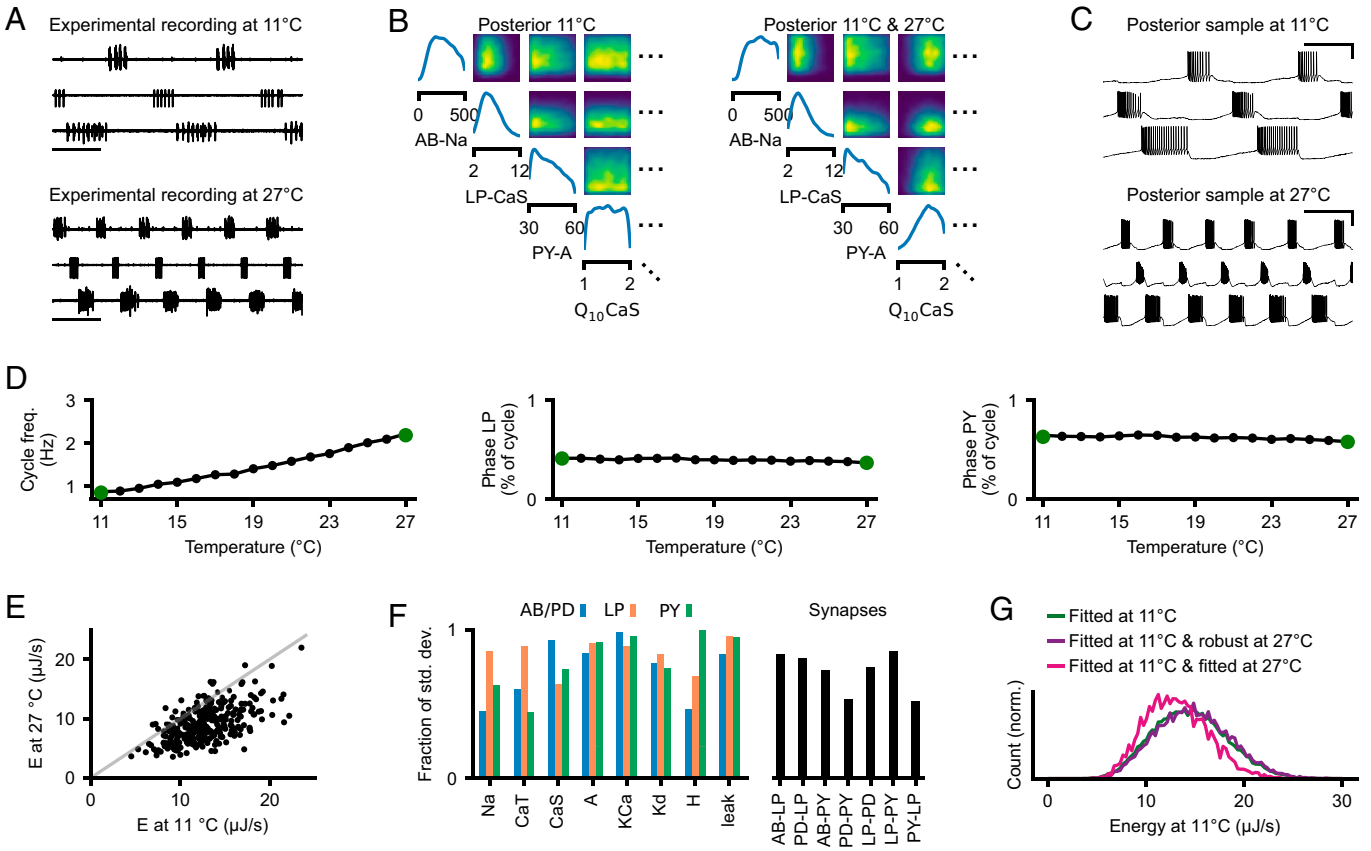

Fig. 7. Temperature robustness does not preclude energy efficiency. (*A*) (*Top*) Experimental data at 11 °C. (*Bottom*) Experimental data at 27 °C (38). (*B*) (*Left*) Posterior distribution given experimental data at 11 °C. (*Right*) Posterior distribution given experimental data at 11 and 27 °C. (*C*) Simulations for a parameter set drawn from the posterior distribution matching experimental data at (*Top*) 11 °C and (*Bottom*) 27 °C. (*D*) (*Left*) Cycle frequency, (*Middle*) phase of LP neuron, and (*Right*) phase of PY neuron for parameter set shown in *C*, simulated at temperatures between 11 and 27 °C. Green dots are the values of the experimental preparations. (*E*) Energy consumption at 11 °C versus 27 °C (time averaged) for 967 circuits sampled from the posterior (in *B*, *Right*). The identity line is shown in gray. (*F*) SD of parameters for models that match experimental data at 11 and 27 °C and that have energy consumption in the lowest 2% quantile at 11 and 27 °C. SD is normalized to the SD of the parameters across all 35,939 models in our database. (*G*) Distribution of the energy consumption of circuits matching experimental data at 11 °C (green), distribution of the energy consumption of circuits that match data at 11 °C and are robust at 27 °C (purple), and distribution of the energy consumption of circuits that match experimental data at 11 and 27 °C (pink).

of neural systems, i.e., the ability to generate similar activity from disparate parameters, confers a certain degree of robustness to such perturbations (7–10, 42, 43). However, not all system configurations might be equally desirable, with some configurations being more energy efficient than others (15). Here we analyzed the energy consumption of parameter configurations with similar activity in the pyloric network of the stomatogastric ganglion. We found that even when the network activity is narrowly tuned to experimental data, the energy consumption can strongly vary between parameter configurations. Despite this diversity of metabolic costs, energy-efficient activity could be produced from a wide range of circuit parameters. When characterizing the range of data-consistent parameters, we found a linear relationship between circuit parameters and energy consumption, which allowed us to identify tuning mechanisms for low energy consumption. Last, we showed that temperature robustness does not preclude energy efficiency and that parameter degeneracy remains despite metabolic and temperature constraints. These findings were facilitated by a methodological advance that increased the efficiency of previously published tools for simulation-based inference (14, 31, 44, 45).

Parameter Degeneracy under Multiple Constraints. In addition to a specific activity, neural circuits are likely constrained by other requirements, e.g., low energy consumption or robustness to perturbations such as fluctuations in temperature or pH (35, 40, 41, 46–50). Here we investigated how energy efficiency impacts the parameter degeneracy of neural systems. While a plausible hypothesis would have been that energy efficiency reduces or eliminates degeneracy altogether, here we found that parameter degeneracy is preserved, even within circuits with very low energy consumption. We identified multiple parameter directions that influence energy consumption only weakly, thus allowing systems to produce energy-efficient network activity with widely disparate circuit parameters. However, we also showed that there are directions in parameter space which drastically impact energy consumption and that changes along these directions lead to configurations which can differ almost by an order of magnitude in their energy consumption. Our results, thus, suggest that changes of most parameters only weakly affect energy consumption, yet some parameters are crucial and should be tuned to achieve low energy consumption.

In our work, parameter degeneracy consisted in the range of pyloric network models that match specific features of experimental activity. We used the same features as in previous work (5), which are physiological constraints of the pyloric network, e.g., cycle duration, burst durations, and gaps and phases of bursts. However, we cannot discard the possibility that the inclusion of additional data features (e.g., spike height or spike width) would have impacted parameter degeneracy and consequently also the range of energies.

Previous work demonstrated that multiple parameter sets in a model of the AB/PD neuron are temperature robust (40).

Downloaded from https://www.pnas.org by MAX-PLANCK-INSTITUT - FUER on January 24, 2023 from IP address 195.37.61.2.

Here we investigated the interplay between energy consumption and temperature robustness at the circuit level and showed that functional, energy-efficient, and temperature-robust activity can be generated from disparate circuit parameters. In addition, consistent with previous work in a single-neuron model of the grasshopper (28), we found that temperature robustness does not require an increased metabolic cost. Whether these results will generalize with the inclusion of the robustness to additional external perturbations, e.g., pH fluctuations (49, 51), or internal perturbations, e.g., neuromodulation (39), remains a subject for future work.

O'Leary and Marder (48) have demonstrated in a model of the PD neuron that some physiological features (such as duty cycle) can be maintained under temperature perturbations when conductances are scaled by a common factor. We tested the possibility that such invariance under conductance scaling could explain the parameter degeneracy and ranges of energies observed in our circuit model: scaling the conductances by a common factor would scale the currents and thereby the energy consumption. However, for the parameter ranges we used [similar ranges as in Prinz et al. (5)], scaling the conductances changed physiological features (such as the cycle duration) of the pyloric rhythm and led to the model not fitting the experimental data accurately (*SI Appendix*, Fig. S25).

More generally, whether there is potential for a system to exhibit parameter degeneracy depends on the number of constraints on the system relative to the number of free parameters: in an overparameterized system, if there is any parameter setting which satisfies the constraints, it is expected that there will be multiple such settings. Our model has 31 conductances and 10 Q_{10} values, and we use 18 voltage features at 11 °C, one energy consumption constraint, and 18 voltage features at 27°. While there is a similar number of constraints relative to the parameter dimensionality, some of those constraints are likely redundant, in which case we have fewer constraints than parameters. Thus, the fact that there are multiple feasible parameter settings is not surprising per se. However, rather than these multiple solutions corresponding to similar parameter values, we found these to be quite disparate in the parameter space.

Relation to Previous Work on Metabolic Cost of Neural Systems. There has been extensive work on quantifying the metabolic cost of biophysical processes in single neurons (15, 22–26) and how single neurons subject to functional constraints can be tuned to minimize energy consumption (15, 16, 23, 25). Consistent with this work, we found that total energy consumption of the pyloric network is strongly influenced by the sodium current (25) but also by the transient and slow calcium currents. The maximal sodium conductance is the most prominent driver of the energy per spike: increases in the conductance lead to an increase of metabolic cost per spike (15, 25). In contrast, calcium currents influence energy consumption through the number of spikes within a burst, despite not consuming much energy themselves. Our results suggest that the maximal conductances of sodium and calcium might be regulated for metabolic efficiency. We thus predict that these conductances are less variable in nature than expected by computational models only matching network activity. Nevertheless, we should note that our findings are based on two simplifying assumptions: first, we studied simple single-compartment neurons rather than more realistic multicompartment neuron models (52), and second, the energy measure is derived directly from the Hodgkin–Huxley model (36), rather than taking into account all the complexity of the ionic exchange leading to ATP consumption (15, 21, 23, 25).

While our study characterizes which parameter configurations are energy efficient, we did not study the mechanisms of how biological circuits would modulate their conductances in order to arrive at these configurations. Long-term changes in intracellular calcium have been found to regulate many ion channels (53–55); thus, it is possible that intracellular calcium is used to tune conductances for energy efficiency. In our study, we found that intracellular calcium level is linearly related to energy consumption across circuit configurations that match experimental data (*SI Appendix*, Fig. S26). It is, therefore, conceivable that the intracellular calcium concentration is used as a rough estimate of the energy consumption and as a feedback signal to tune membrane and synaptic conductances into energy-efficient regimes, subject to additional constraints such as functional activity and robustness to various perturbations (55).

Previous studies have demonstrated that synaptic mechanisms can consume a substantial amount of energy (21, 56, 57). In contrast, in the considered model of the pyloric network, synaptic currents consume only a minor fraction of energy [∼0.08% of the total energy is consumed by synapses, whereas Attwell and Laughlin (21) report 40% of energy being consumed by synaptic mechanisms]. A potential reason for this difference is the low number of connections in our model of the pyloric network: each model neuron projects to up to three other model neurons, whereas the synaptic energy consumption reported in Attwell and Laughlin (21) is based on the assumption of 8,000 synaptic boutons per neuron. Cabirol-Pol et al. (58) report only few synaptic sites between the PD and LP neuron in the lobster *Homarus gammarus*. Thus, models of more complex neural circuits driven by excitatory, recurrent connectivity, such as the ones found in the cortex, might spend a larger fraction of energy on synaptic mechanisms.

We used a measure of energy consumption that is based on an equivalent electrical circuit. This measure ignores a range of internal processes taking place within biological neurons, e.g., the efficiency of ion pumps or the vesicle release at synapses (21), and, therefore, underestimates the true energy consumption of the biological circuit. We reproduced our main results for a current-based energy measure taking into account the efficiency of pumps (*SI Appendix*, Fig. S3). While the absolute values of the energy consumption changed (see different ranges of energy in *SI Appendix*, Fig. S3 *A* and *D* as compared to Figs. 2*H* and 7*G*), the results are highly similar due to the proportionality between the two measures ($\rho = 0.999$; *SI Appendix*, Figs. S1 and S2). In addition, a more detailed model of synaptic energy consumption (including, e.g., vesicle release) would likely change the cost of synaptic activity, although synaptic cost constitutes only a very small fraction (0.08%) of total energy consumption in our circuit model. It is, thus, unlikely that the use of synapses with more biophysical details would entirely change the conclusions of our study. Additional factors such as glutamate recycling, presynaptic Ca^{2+} entry, and maintaining resting potentials would also modify our estimate of the energy consumption, but these factors are reported to consume a rather small fraction (<20%) of energy expenditure in the brain (21).

Energy Efficiency in the Pyloric Network. Experimental studies have shown that the parameters of the pyloric network vary across wide ranges (1, 2, 59). This raises the question of whether these disparate solutions are all tuned for energy efficiency. In our study, we demonstrated that energy-efficient circuit function can be compatible with many parameter configurations. Therefore, despite the variability of the parameters, each configuration in the crab *C. borealis* might be tuned for low energy consumption.

Downloaded from https://www.pnas.org by MAX-PLANCK-INSTITUT - FUER on January 24, 2023 from IP address 195.37.61.2.

However, the pyloric network is a small subset of the nervous system of the crab and, therefore, likely consumes a small fraction of its total energy budget. Thus, even if the nervous system of the crab is tuned for energy efficiency, it could still achieve this without strict energy requirements for the pyloric network.

Increasing the Efficiency of Simulation-Based Inference. We used a previously introduced tool, SNPE (14, 45), to identify all models consistent with experimentally measured activity as well as prior knowledge about realistic parameter ranges. We improved the efficiency of SNPE by introducing a classifier that rejects invalid simulations (31). By using this classifier, we were able to improve the accuracy of SNPE while requiring only half as many simulations (14). Because of this larger simulation budget, the resulting posterior distributions became more accurate. Furthermore, the trained neural density estimator is amortized; i.e., one can obtain the posterior distribution for multiple experimental preparations without running further simulations or training a new neural network.

The classifier-enhanced SNPE can be applied to other modeling studies in neuroscience. In particular, the classifier to predict invalid simulations is valuable whenever there are parameter values for which the computational model of interest produces ill-defined features: e.g., the spike shape cannot be defined in cases where a neuron model does not produce spikes. Our method has the potential to significantly speed up inference in these scenarios.

Implications for the Operation of Neural Circuits. Our findings suggest that neural circuits can be energy efficient with largely disparate biophysical parameters, even with highly specific functional requirements under naturally occurring perturbations. This raises the question of whether such energy efficiency is present in real biological systems and how these systems could be tuned for metabolic efficiency.

Materials and Methods

Code to reproduce the figures is available at https://github.com/mackelab/stg_energy. Code for running SNPE and training a classifier to reject invalid simulations is available in our toolbox: https://github.com/mackelab/sbi (60). A tutorial for how to use these features can be found on our website: https://www.mackelab.org/sbi. The simulator of the pyloric network in Cython (61) is available at https://github.com/mackelab/pyloric.

We analyzed extracellular recordings of the stomatogastric motor neurons that are involved in the triphasic pyloric rhythm in the crab *C. borealis* (38, 39). The circuit model of the crustacean stomatogastric ganglion was adapted from Prinz et al. (5). To compute the energy consumption of a specific network activity, we followed the approach of Moujahid et al. (36). In order to find circuit models that are consistent with the neural data, we used an extension of SNPE (14). Further details about the data, modeling, and inference are available in *SI Appendix*, SI Text.

Data, Materials, and Software Availability. Computer code has been deposited in GitHub (https://github.com/mackelab/stg_energy) (62). Previously published data were used for this work (38).

ACKNOWLEDGMENTS. We thank Sara A. Haddad and Eve Marder for sharing their data and discussions; Martin Stemmler for discussions; and Poornima Ramesh, Richard Gao, and Jan Boelts for discussions and comments on the manuscript. We also thank the reviewers for a constructive review process which significantly improved the manuscript. M.D. is supported by the International Max Planck Research School for Intelligent Systems. This work was supported by the German Research Foundation through Sonderforschungsbereich (SFB) 1089 "Synaptic Microcircuits" and Germany's Excellence Strategy–EXC-Number 2064/1, project 390727645, as well as the German Federal Ministry of Education and Research (project ADIMEM, FKZ 01IS18052 A-D and Tübingen AI Center, FKZ 01IS18039A).

Author affiliations: [a]Machine Learning in Science, Excellence Cluster "Machine Learning," Tübingen University, 72076 Tübingen, Germany; [b]Max Planck Institute for Intelligent Systems, Department of Empirical Inference, 72076 Tübingen, Germany; and [c]Max Planck Institute for Neurobiology of Behavior – caesar, 53175 Bonn, Germany

1. J. Golowasch, L. F. Abbott, E. Marder, Activity-dependent regulation of potassium currents in an identified neuron of the stomatogastric ganglion of the crab Cancer borealis. *J. Neurosci.* **19**, RC33 (1999).
2. J. Golowasch, M. S. Goldman, L. F. Abbott, E. Marder, Failure of averaging in the construction of a conductance-based neuron model. *J. Neurophysiol.* **87**, 1129–1131 (2002).
3. M. S. Goldman, J. Golowasch, E. Marder, L. F. Abbott, Global structure, robustness, and modulation of neuronal models. *J. Neurosci.* **21**, 5229–5238 (2001).
4. A. A. Prinz, C. P. Billimoria, E. Marder, Alternative to hand-tuning conductance-based models: Construction and analysis of databases of model neurons. *J. Neurophysiol.* **90**, 3998–4015 (2003).
5. A. A. Prinz, D. Bucher, E. Marder, Similar network activity from disparate circuit parameters. *Nat. Neurosci.* **7**, 1345–1352 (2004).
6. R. C. Roffman, B. J. Norris, R. L. Calabrese, Animal-to-animal variability of connection strength in the leech heartbeat central pattern generator. *J. Neurophysiol.* **107**, 1681–1693 (2012).
7. G. M. Edelman, J. A. Gally, Degeneracy and complexity in biological systems. *Proc. Natl. Acad. Sci. U.S.A.* **98**, 13763–13768 (2001).
8. E. Marder, A. L. Taylor, Multiple models to capture the variability in biological neurons and networks. *Nat. Neurosci.* **14**, 133–138 (2011).
9. J. N. MacLean, Y. Zhang, B. R. Johnson, R. M. Harris-Warrick, Activity-independent homeostasis in rhythmically active neurons. *Neuron* **37**, 109–120 (2003).
10. J. N. MacLean *et al.*, Activity-independent coregulation of IA and Ih in rhythmically active neurons. *J. Neurophysiol.* **94**, 3601–3617 (2005).
11. R. N. Gutenkunst *et al.*, Universally sloppy parameter sensitivities in systems biology models. *PLOS Comput. Biol.* **3**, 1871–1878 (2007).
12. R. Grashow, T. Brookings, E. Marder, Compensation for variable intrinsic neuronal excitability by circuit-synaptic interactions. *J. Neurosci.* **30**, 9145–9156 (2010).
13. T. O'Leary, A. C. Sutton, E. Marder, Computational models in the age of large datasets. *Curr. Opin. Neurobiol.* **32**, 87–94 (2015).
14. P. J. Gonçalves *et al.*, Training deep neural density estimators to identify mechanistic models of neural dynamics. *eLife* **9**, e56261 (2020).
15. A. Hasenstaub, S. Otte, E. Callaway, T. J. Sejnowski, Metabolic cost as a unifying principle governing neuronal biophysics. *Proc. Natl. Acad. Sci. U.S.A.* **107**, 12329–12334 (2010).
16. B. Sengupta, A. A. Faisal, S. B. Laughlin, J. E. Niven, The effect of cell size and channel density on neuronal information encoding and energy efficiency. *J. Cereb. Blood Flow Metab.* **33**, 1465–1473 (2013).
17. B. Sengupta, M. B. Stemmler, Power consumption during neuronal computation. *Proc. IEEE* **102**, 738–750 (2014).
18. J. Astrup, P. M. Sørensen, H. R. Sørensen, Oxygen and glucose consumption related to Na+-K+ transport in canine brain. *Stroke* **12**, 726–730 (1981).
19. J. Astrup, P. M. Sørensen, H. R. Sørensen, Inhibition of cerebral oxygen and glucose consumption in the dog by hypothermia, pentobarbital, and lidocaine. *Anesthesiology* **55**, 263–268 (1981).
20. L. Sokoloff, Energetics of functional activation in neural tissues. *Neurochem. Res.* **24**, 321–329 (1999).
21. D. Attwell, S. B. Laughlin, An energy budget for signaling in the grey matter of the brain. *J. Cereb. Blood Flow Metab.* **21**, 1133–1145 (2001).
22. H. Alle, A. Roth, J. R. Geiger, Energy-efficient action potentials in hippocampal mossy fibers. *Science* **325**, 1405–1408 (2009).
23. M. B. Stemmler, B. Sengupta, S. Laughlin, J. Niven, "Energetically optimal action potentials" in *Advances in Neural Information Processing Systems*, J. Shawe-Taylor, R. Zemel, P. Bartlett, F. Pereira, K. Q. Weinberger, Eds. (Curran Associates, Inc., 2011), pp. 1566–1574.
24. B. C. Carter, B. P. Bean, Sodium entry during action potentials of mammalian neurons: Incomplete inactivation and reduced metabolic efficiency in fast-spiking neurons. *Neuron* **64**, 898–909 (2009).
25. B. Sengupta, M. Stemmler, S. B. Laughlin, J. E. Niven, Action potential energy efficiency varies among neuron types in vertebrates and invertebrates. *PLOS Comput. Biol.* **6**, e1000840 (2010).
26. G. Yi, Y. Fan, J. Wang, Metabolic cost of dendritic Ca^{2+} action potentials in layer 5 pyramidal neurons. *Front. Neurosci.* **13**, 1221 (2019).
27. S. Onasch, J. Gjorgjieva, Circuit stability to perturbations reveals hidden variability in the balance of intrinsic and synaptic conductances. *J. Neurosci.* **40**, 3186–3202 (2020).
28. F. A. Roemschied, M. J. Eberhard, J. H. Schleimer, B. Ronacher, S. Schreiber, Cell-intrinsic mechanisms of temperature compensation in a grasshopper sensory receptor neuron. *eLife* **3**, e02078 (2014).
29. R. M. Harris-Warrick *et al.*, *Dynamic Biological Networks: The Stomatogastric Nervous System* (MIT Press, 1992).
30. E. Marder, D. Bucher, Understanding circuit dynamics using the stomatogastric nervous system of lobsters and crabs. *Annu. Rev. Physiol.* **69**, 291–316 (2007).
31. J. M. Lueckmann *et al.*, "Flexible statistical inference for mechanistic models of neural dynamics" in *Advances in Neural Information Processing Systems*, I. Guyon *et al.*, Eds. (Curran Associates, Inc., 2017), pp. 1289–1299.
32. L. Stehlik, C. MacKenzie Jr., W. Morse, Distribution and abundance of four brachyuran crabs on the northwest Atlantic shelf. *Fish Bull.* **89**, 473–492 (1991).
33. M. J. Donahue *et al.*, Predation risk, prey abundance, and the vertical distribution of three brachyuran crabs on Gulf of Maine shores. *J. Crustac. Biol.* **29**, 523–531 (2009).
34. C. J. Krediet, M. J. Donahue, Growth-mortality trade-offs along a depth gradient in cancer borealis. *J. Exp. Mar. Biol. Ecol.* **373**, 133–139 (2009).
35. L. S. Tang *et al.*, Precise temperature compensation of phase in a rhythmic motor pattern. *PLoS Biol.* **8**, e1000469 (2010).
36. A. Moujahid, A. d'Anjou, F. J. Torrealdea, F. Torrealdea, Energy and information in Hodgkin-Huxley neurons. *Phys. Rev. E Stat. Nonlin. Soft Matter Phys.* **83**, 031912 (2011).

Downloaded from https://www.pnas.org by MAX-PLANCK-INSTITUT - FUER on January 24, 2023 from IP address 195.37.61.2.

37. L. M. Alonso, E. Marder, Visualization of currents in neural models with similar behavior and different conductance densities. *eLife* **8**, e42722 (2019).
38. S. A. Haddad, E. Marder, Recordings from the *C. borealis* stomatogastric nervous system at different temperatures in the decentralized condition (2021). https://doi.org/10.5281/zenodo.5139650. Accessed 1 August 2021.
39. S. A. Haddad, E. Marder, Circuit robustness to temperature perturbation is altered by neuromodulators. *Neuron* **100**, 609–623.e3 (2018).
40. J. S. Caplan, A. H. Williams, E. Marder, Many parameter sets in a multicompartment model oscillator are robust to temperature perturbations. *J. Neurosci.* **34**, 4963–4975 (2014).
41. L. M. Alonso, E. Marder, Temperature compensation in a small rhythmic circuit. *eLife* **9**, e55470 (2020).
42. E. Marder, Variability, compensation, and modulation in neurons and circuits. *Proc. Natl. Acad. Sci. U.S.A.* **108** (suppl. 3), 15542–15548 (2011).
43. E. Marder, M. L. Goeritz, A. G. Otopalik, Robust circuit rhythms in small circuits arise from variable circuit components and mechanisms. *Curr. Opin. Neurobiol.* **31**, 156–163 (2015).
44. G. Papamakarios, T. Pavlakou, I. Murray, "Masked autoregressive flow for density estimation" in *Advances in Neural Information Processing Systems*, I. Guyon *et al.*, Eds. (Curran Associates, Inc., 2017), pp. 2338–2347.
45. D. Greenberg, M. Nonnenmacher, J. Macke, "Automatic posterior transformation for likelihood-free inference" in *International Conference on Machine Learning*, K. Chaudhuri, R. Salakhutdinov, Eds. (PMLR, 2019), pp. 2404–2414.
46. L. S. Tang, A. L. Taylor, A. Rinberg, E. Marder, Robustness of a rhythmic circuit to short- and long-term temperature changes. *J. Neurosci.* **32**, 10075–10085 (2012).
47. A. Rinberg, A. L. Taylor, E. Marder, The effects of temperature on the stability of a neuronal oscillator. *PLOS Comput. Biol.* **9**, e1002857 (2013).
48. T. O'Leary, E. Marder, Temperature-robust neural function from activity-dependent ion channel regulation. *Curr. Biol.* **26**, 2935–2941 (2016).
49. J. A. Haley, D. Hampton, E. Marder, Two central pattern generators from the crab, *Cancer borealis*, respond robustly and differentially to extreme extracellular pH. *eLife* **7**, e41877 (2018).
50. S. Gorur-Shandilya *et al.*, Mapping circuit dynamics during function and dysfunction. *eLife* **11**, e76579 (2022).
51. J. Ratliff, A. Franci, E. Marder, T. O'Leary, Neuronal oscillator robustness to multiple global perturbations. *Biophys. J.* **120**, 1454–1468 (2021).
52. G. Le Masson, S. Przedborski, L. F. Abbott, A computational model of motor neuron degeneration. *Neuron* **83**, 975–988 (2014).
53. M. E. Barish, Intracellular calcium regulation of channel and receptor expression in the plasmalemma: Potential sites of sensitivity along the pathways linking transcription, translation, and insertion. *J. Neurobiol.* **37**, 146–157 (1998).
54. T. O'Leary, M. C. van Rossum, D. J. Wyllie, Homeostasis of intrinsic excitability in hippocampal neurones: Dynamics and mechanism of the response to chronic depolarization. *J. Physiol.* **588**, 157–170 (2010).
55. T. O'Leary, A. H. Williams, A. Franci, E. Marder, Cell types, network homeostasis, and pathological compensation from a biologically plausible ion channel expression model. *Neuron* **82**, 809–821 (2014).
56. W. B. Levy, R. A. Baxter, Energy-efficient neuronal computation via quantal synaptic failures. *J. Neurosci.* **22**, 4746–4755 (2002).
57. B. Sengupta, M. B. Stemmler, K. J. Friston, Information and efficiency in the nervous system–A synthesis. *PLOS Comput. Biol.* **9**, e1003157 (2013).
58. M. J. Cabirol-Pol, D. Combes, V. S. Fénelon, J. Simmers, P. Meyrand, Rare and spatially segregated release sites mediate a synaptic interaction between two identified network neurons. *J. Neurobiol.* **50**, 150–163 (2002).
59. D. J. Schulz, J. M. Goaillard, E. Marder, Variable channel expression in identified single and electrically coupled neurons in different animals. *Nat. Neurosci.* **9**, 356–362 (2006).
60. A. Tejero-Cantero *et al.*, sbi: A toolkit for simulation-based inference. *J. Open Source Softw.* **5**, 2505 (2020).
61. S. Behnel *et al.*, Cython: The best of both worlds. *Comput. Sci. Eng.* **13**, 31–39 (2010).
62. M. Deistler, J. H. Macke, P. J. Goncalves, Code for "Energy-efficient network activity from disparate circuit parameters." GitHub. https://github.com/mackelab/stg_energy. Deposited 30 August 2020.

Downloaded from https://www.pnas.org by MAX-PLANCK-INSTITUT - FUER on January 24, 2023 from IP address 195.37.61.2.